American Journal of Engineering Research (AJER)
e-ISSN: 2320-0847 p-ISSN : 2320-0936
Volume-12, Issue-4, pp-33-41
www.ajer.org
Research Paper Open Access

Modeling Of Walking Behavior in Load of the Asynchronous Cage Motor of the Carrigres Crushing

Kabimba Mupa [1], Lidinga Mobonda Flory [2], Messo Léonide [3], Meni Babakidi Narcisse[4], Bandekela Kazadi André [5], Lilonga Boyenga Désiré [6].

Abstract: This article that we present will approach the model of the electric control of the asynchronous motor with universal cage; among the control techniques of the asynchronous machine by acting on the slip, it is possible to regulate the speed of the asynchronous cage motor directly by the voltage and the frequency. The need for static converters is justified by the fact that: the role of the rectifier is to rectify the three-phase voltages, and the non-autonomous inverter (frequency conversion) is responsible for converting voltage and frequency.
The objective of this article is to describe the behavior of the cage asynchronous motor by a mathematical model based on the nonlinear equations of the electromechanical quantities of the motor facilitate the evaluation of the performances of the motor. These models confirm that the variation of the speed of the asynchronous motor is closely linked to the power of the converter associated with the stator.
Keywords: Modeling, Behavior, Running under load, Asynchronous squirrel cage motor, Crushing.

Date of Submission: 01-04-2023 Date of acceptance: 11-04-2023

I.INTRODUCTION

Modeling consists in putting into equation the different parameters of a system. At the end of this operation we are faced with the following problem: the more the model approaches reality, the more it becomes complex and requires a very important means of calculation, on the other hand if the system is simplified, the calculations become easy but we are moving away from reality. A judicious choice consists in idealizing the machine and consequently keeping the most important phenomena and neglecting the secondary phenomena. It is therefore important that the model be usable in both static and dynamic regimes. To do this we must resort to simplifying assumptions on which our study will be based. The machine being a non-linear system, it is necessary to have a model faithfully representing its behavior at the level of its electrical, electromagnetic and mechanical models**.**

II. DYNAMIC MODEL OF THE ASYNCHRONOUS MACHINE

II.1 Three-phase asynchronous machine

The three-phase asynchronous machine is shown schematically in Figure. II.1. It has six windings. The stator of the machine is made up of three fixed windings offset by 120° in space and traversed by three variable currents. The rotor can be modeled by three identical windings staggered in space by 120°. These windings are short-circuited and the voltage across them is zero.

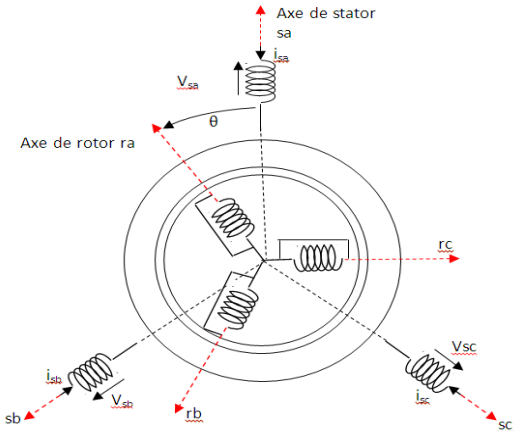

Fig. II.1: Schematic of a machine

II.1.1 Electrical equations

Applying the generalized Ohm's law to each winding of the machine gives the stator and rotor voltage equations as follows:

$$\begin{bmatrix} V_{as} \\ V_{bs} \\ V_{cs} \end{bmatrix} = \begin{bmatrix} R_s & 0 & 0 \\ 0 & R_s & 0 \\ 0 & 0 & R_s \end{bmatrix} . \begin{bmatrix} I_{as} \\ I_{bs} \\ I_{cs} \end{bmatrix} + \frac{d}{dt} \begin{bmatrix} \phi_{as} \\ \phi_{bs} \\ \phi_{cs} \end{bmatrix} \quad (2.1)$$

The rotor voltage equations can be expressed by:

$$\begin{bmatrix} 0 \\ 0 \\ 0 \end{bmatrix} = \begin{bmatrix} R_r & 0 & 0 \\ 0 & R_r & 0 \\ 0 & 0 & R_r \end{bmatrix} . \begin{bmatrix} I_{ar} \\ I_{br} \\ I_{cr} \end{bmatrix} + \frac{d}{dt} \begin{bmatrix} \phi_{ar} \\ \phi_{br} \\ \phi_{cr} \end{bmatrix} \quad (2.2)$$

II.1.2 Magnetic equations

The simplifying assumptions cited above give linear relations between the fluxes and the currents of the machine, which are written in matrix form as follows:

$$\begin{bmatrix} \Phi_{as} \\ \Phi_{bs} \\ \Phi_{cs} \end{bmatrix} = \begin{bmatrix} l_s & M_s & M_s \\ M_s & l_s & M_s \\ M_s & M_s & l_s \end{bmatrix} . \begin{bmatrix} I_{as} \\ I_{bs} \\ I_{cs} \end{bmatrix} + [MO] \begin{bmatrix} \cos\theta & \cos(\theta + \frac{2\pi}{3}) & \cos(\theta - \frac{2\pi}{3}) \\ \cos(\theta - \frac{2\pi}{3}) & \cos\theta & \cos(\theta + \frac{2\pi}{3}) \\ \cos(\theta + \frac{2\pi}{3}) & \cos(\theta - \frac{2\pi}{3}) & \cos\theta \end{bmatrix} . \begin{bmatrix} I_{ar} \\ I_{br} \\ I_{cr} \end{bmatrix} \quad (2.3)$$

$$\begin{bmatrix} \Phi_{ar} \\ \Phi_{br} \\ \Phi_{cr} \end{bmatrix} = \begin{bmatrix} l_r & M_r & M_r \\ M_r & l_r & M_r \\ M_r & M_r & l_r \end{bmatrix} . \begin{bmatrix} I_{ar} \\ I_{br} \\ I_{cr} \end{bmatrix} + MO \begin{bmatrix} \cos\theta & \cos(\theta - \frac{2\pi}{3}) & \cos(\theta + \frac{2\pi}{3}) \\ \cos(\theta + \frac{2\pi}{3}) & \cos\theta & \cos(\theta - \frac{2\pi}{3}) \\ \cos(\theta - \frac{2\pi}{3}) & \cos(\theta + \frac{2\pi}{3}) & \cos\theta \end{bmatrix} . \begin{bmatrix} I_{as} \\ I_{bs} \\ I_{cs} \end{bmatrix} \quad (2.4)$$

II.1.3 Equation of motion

To have a complete model of the machine. It is necessary to introduce the mechanical parameters (torque, speed, etc.). The expression describing the dynamics of the moving part of the machine is expressed by the following equation of motion:

$$j\frac{d\Omega}{dt} + f\Omega = C_e - C_r \quad (2.5)$$

We then use mathematical transformations which make it possible to describe the behavior of the machine using differential equations with constant coefficients. The transformations used must preserve the instantaneous power and the reciprocity of the mutual inductances. This makes it possible to establish an expression of the electromagnetic torque in the frame corresponding to the transformed system and which remains valid for the real machine.

II. 2 Engine parameter equations

II.2.1 Determination of stator joule losses

The stator joule losses in a three-phase machine are obtained by the expression:

$$P_{jst} = 3R.I_{ph}^2 \quad (2.6)$$

$$R_s = \frac{U}{I_{ph}} \quad (2.7)$$

II.2.2 Variation of the resistance of the stator windings

We have the stator joule losses in a three-phase machine, for an unstable regime, this loss will be obtained by the following expression:

$$R_s = \frac{U}{I_{ph}} \quad (2.8)$$

II.2.3 Torque equations as a function of voltage

$$\mathrm{C_m} = \mathrm{k.U^2} \quad (2.9)$$

II.2.4 Torque equations as a function of absorbed current

The torque as a function of the current is obtained by the following expression

$$\mathrm{C_m} = \mathrm{k}.C_{st} \quad (2.10)$$

II.2.5 Determination of mechanical parameters: J , f

The identification of the mechanical parameters J and f (moment of inertia and coefficient of viscous friction respectively) is based on the measurement of the mechanical losses when the machine rotates at a given speed and is done by measuring the speed as a function of time during the slow-down. The moment of inertia J can be calculated by:

$$J = \frac{P_{méc}}{\Omega_n \left(\frac{d\Omega}{dt}\right)_{\Omega=\Omega s}} (2.6)$$

This relation shows that the measurement of the moment of inertia J depends on the precision with which the mechanical power is determined. Reading the deceleration curve and its approximation by an analytical function makes it possible to calculate the derivative of the speed:

$$\frac{d\Omega}{dt} = 2\pi \frac{\Delta N}{\Delta t} \frac{1}{60} (2.11)$$

$$\Omega_n = 2\pi \frac{N_n}{60} (2.12)$$

III. LOAD TEST

III.1 Current measurement

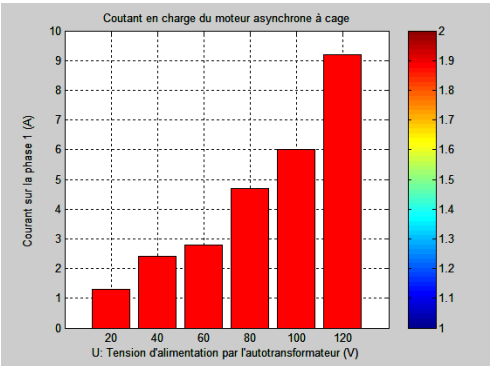

Figure III.1: Current on phase 1

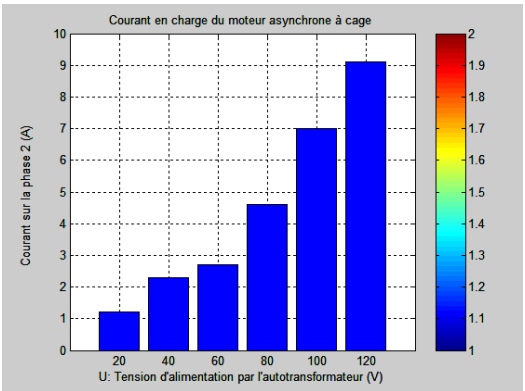

Figure III.2: Phase 2 current

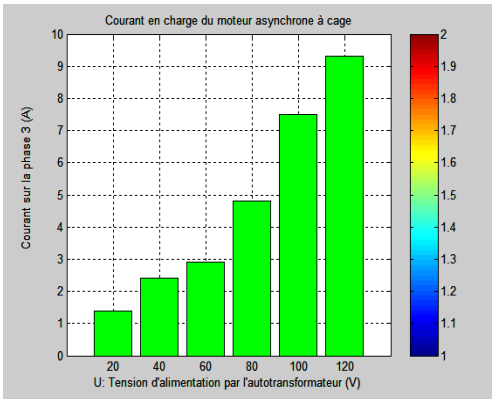

Figure III.3: Current on phase 3

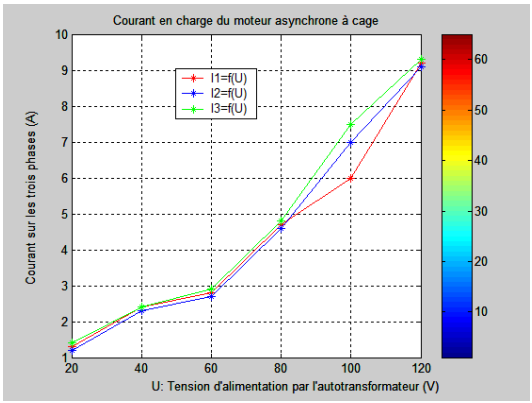

Figure III.4: Current on the phases

The simulation curves give the different points of the currents. The red curve describes the behavior of the current of the first phase, which increases under the interval of 1.3 A up to 9.2 A. The blue curve describes the behavior of the current of the second phase, which increases under the interval of 1.2 A up to 9.1 A. The green curve describes the behavior of the current of the third phase, which increases under the interval of 1.4 A up to 9.3 A. all these currents are function of the variation in the voltage of the autotransformer, within the framework of the load test.

III.1.5 Rated torque

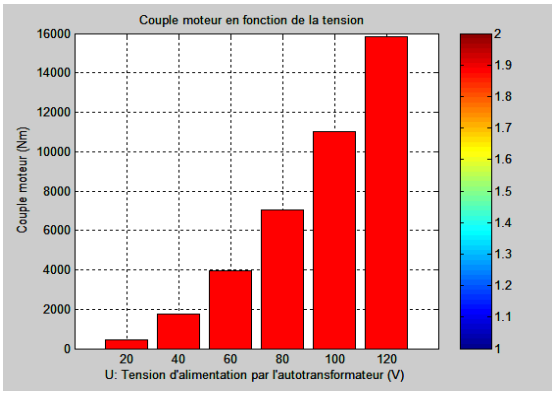

Figure III.19: Engine torque simulation

The shape of the bar is almost rising, this bar describes the evolution of the motor torque as a function of the tension under the interval of 440 Nm up to 15840 Nm. This simulation is taken into account in the load test.

III.1.6 Torque as a function of absorbed current

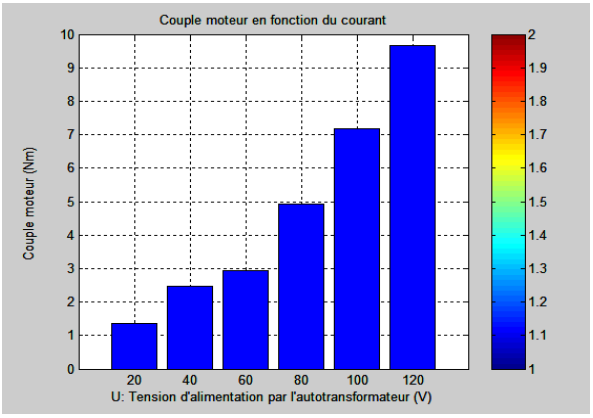

Figure III.20: Simulation of the different engine torques

The simulation bar gives the different points of the motor torques. The blue curve describes the shape of the motor torque in the stator current which increases under the interval of 1.365 Nm up to 9.66 Nm.

III.2 Determination of stator joule losses

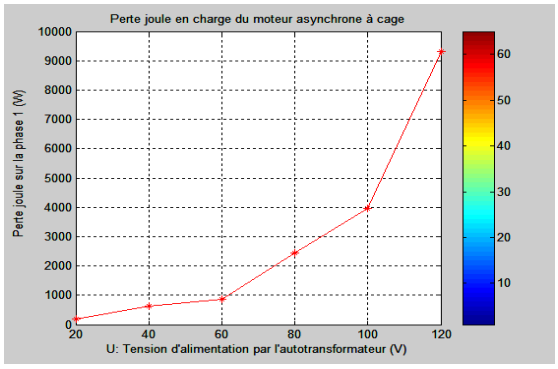

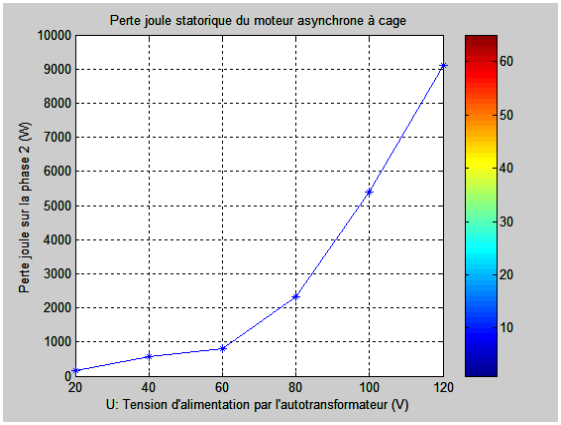

Figure III.10: Determination of the joule losses of phase 1 Figure III.11: Determination of the joule losses of phase 2

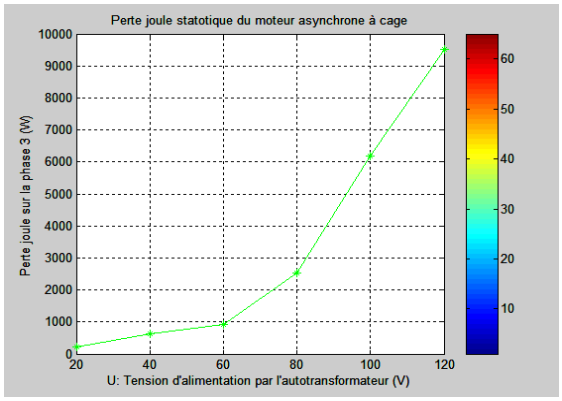

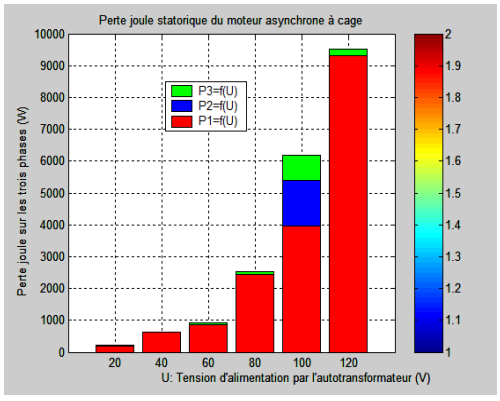

Figure III.12: Determination of the joule losses of phase3 Figure III.13: Determination of Joule losses of three phases

The bars of the simulations give the different points of the joule losses. The red bar depicts the joule loss behavior of the third phase, which grows below the 215.6 W interval to 9513.9 W. The blue bar depicts the joule loss behavior of the second phase, which grows below the 158.4 W interval down to 9109.1 W. The green bar depicts the joule loss behavior of the first phase, which grows below the 185.9 W interval down to 9310.4 W. all these currents are a function of the variation in the voltage of the autotransformer, within the framework of the load test.

III. 3 Variation of the resistance of the stator windings

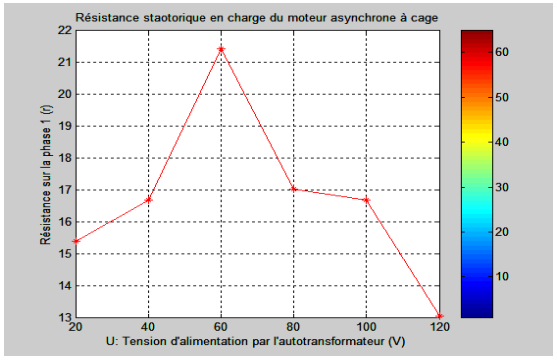

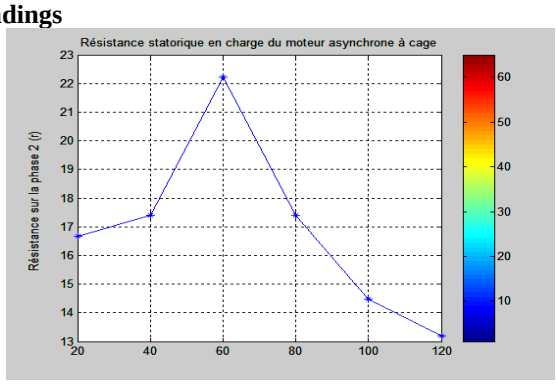

Figure III.10: Determination of resistance on phase 1 Figure III.11: Determination of resistance on phase 2

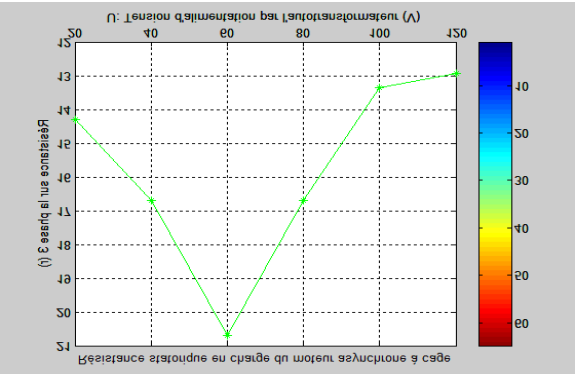

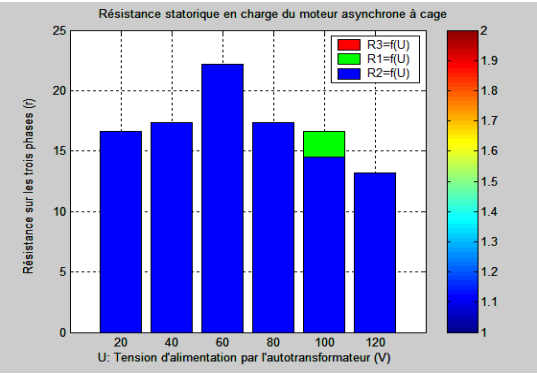

Figure III.13: Determination of the resistance on phase3 Figure III.14: Determination of the resistance on the phases

The simulation bars give the different points of the stator resistances. The red bar describes the resistance behavior on the third phase, which increases under the interval of 33.33 Ω up to 41.37 Ω. The blue bar describes the resistance behavior on the second phase, which increases under the interval of 50 Ω up to 48 Ω. The green bar describes the resistance behavior on the first phase, which increases below the 40 Ω interval up to 42.85 Ω. all these currents are a function of the variation in the voltage of the autotransformer, within the framework of the on-load test.

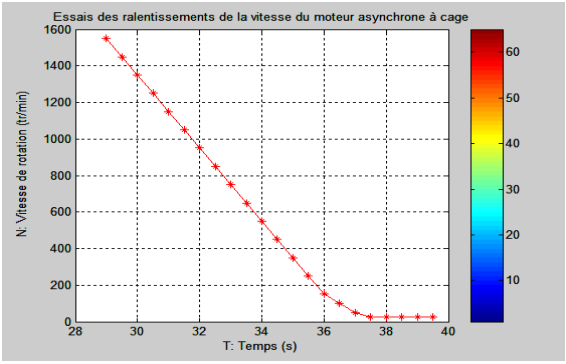

Figure.III.12. MAS Slowdown Tests

IV. LOAD OPERATION

IV.1. Experimental validation of the parameters with a load test

The comparison between the simulated and real values during direct start-up of MAS under load is given by the curves below.

IV.1.1

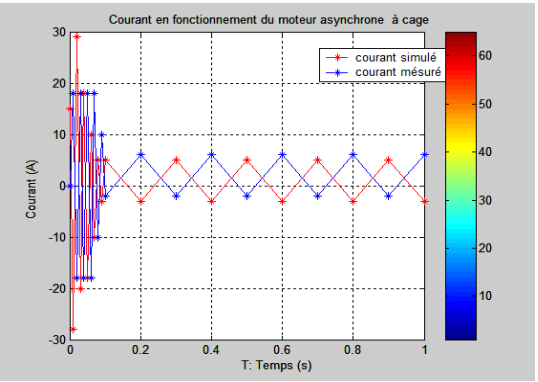

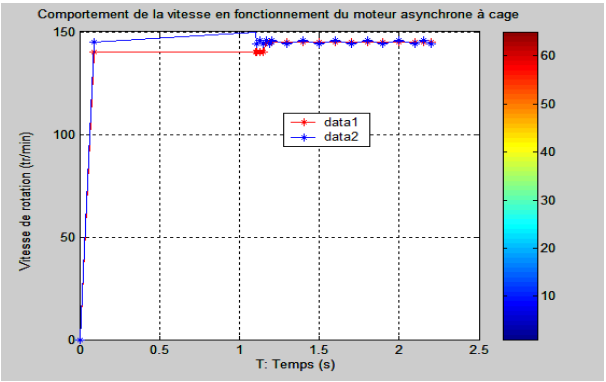

Figure.IV.1: Comparison of currents Figure.IV.2: Comparison of speeds

The comparison of measurements and simulations shows that the identified parameters give good results. We even observe a difference between the current-speed measurements obtained in the validation.

IV.2 Simulation and interpretation of the DFOC command

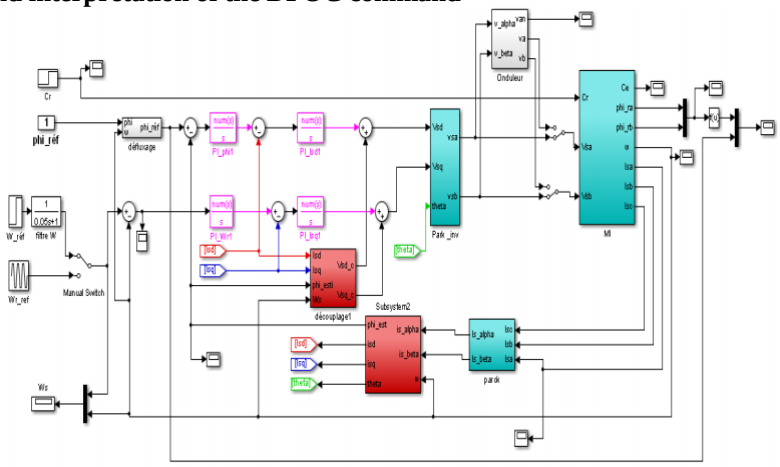

Figure.IV.3. MAS DFOC vector control on Matlab/Simulink.

The simulation results are respectively presented in figures (IV.3 (a), (b), (c) and (d)) for the speed, flux, torque and stator current responses including the errors between the output and setpoint.

IV.2.1 Simulation result

The simulation carried out with a change in the speed setpoint from +140 rad/s to -140 rad/s. under the application of a load torque equal to 6.5 Nm at time 0.9 seconds, figure (IV.4).

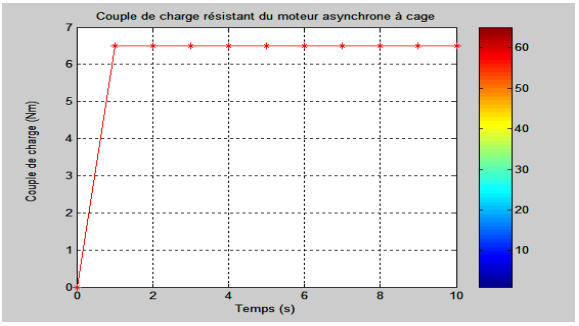

Figure.IV.4.Behavior of the load torque Cr

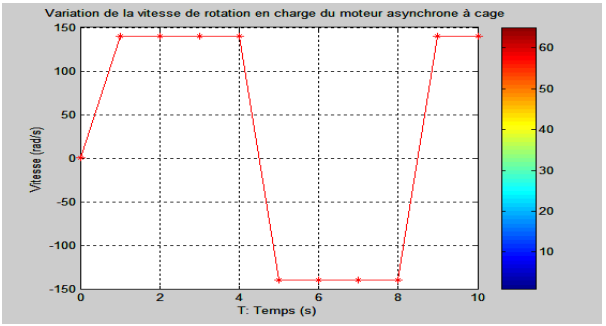

Figure.IV.5.Variation of speed

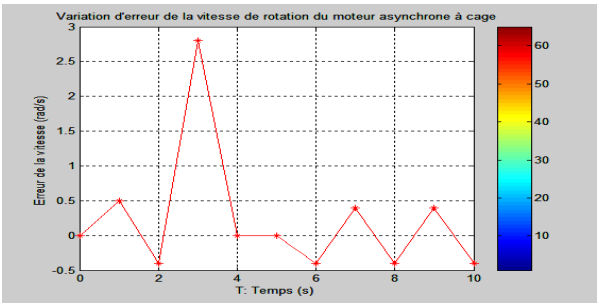

Figure IV.6: Speed error variation

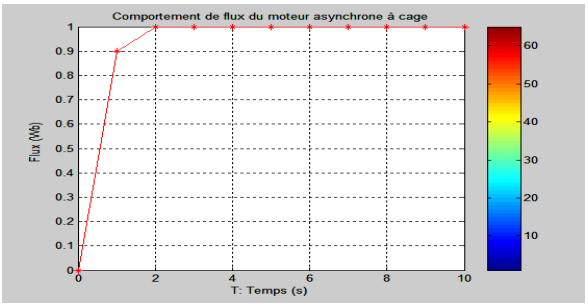

Figure IV.7: Flow variation

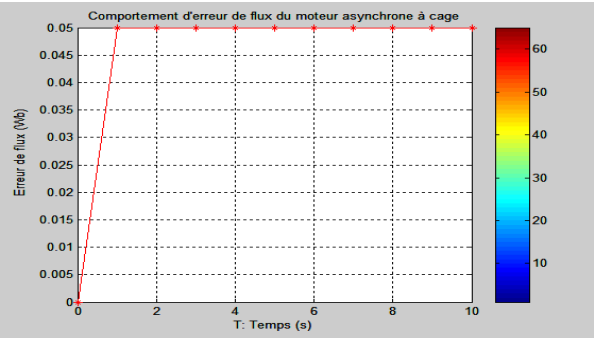

Figure IV.8: Flow error variation

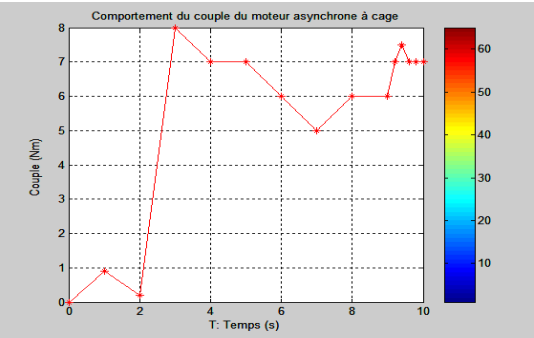

Figure IV.9: Couple behavior

V. CONCLUSION

This article consisted of modeling the control of the Carrigres crushing line using the flux-oriented direct vector control strategy to control the speed and torque of the machine; the objective being to achieve a decoupling of the flux and the torque. The speed variation will indicate that there is a good continuation of its reference value even when reversing the direction of rotation of the speed, but a peak following the application of a load torque equal to 6.5 Nm at time t=0.9s: this is what makes this method not very robust. The rotor flux norm is very close to the reference (i.e. an error of 10-4). Therefore, the motor precisely follows the value of the speed and flux setpoint.

REFERENCE

[1]. A. Dumitrescu, D. Fodor, T. Jokinen, M. Rosu, S. Bucurencio: "Modeling and simulation of electric drive system using Matlab/simulink Environment's", International conference on Electric Machines and Drives (IEMD), 1999 pp. 451-453.
[2]. A. Ba-Razzouk, A. Chériti, and Pierre Sicard, " Implementation of a DSP Based Real-Time Estimator of Induction Motors Rotor Time Constant", IEEE Trans. Power electron.,Vol.17, pp. 534-542, July 2002.
[3]. Ramu Khrisnan, " Electric Motor Drives Modeling, Analysis, and Control ,Virginia Tech, Blacksburg, VA. Prentice Hall, USA, 2001.
[4]. Barra K. and K. Benmahammed, A new extended cascaded predictive control ECGPC of an induction motor drive with energy saving, IEEE Mediterranean Electrotechnical Conference, Benalmaden, Spain, p.p. 1150-1153, 2006
[5]. Naït-Saïd MS, Benbouzid MEH and Benchaid A., "Detection of broken bars induction motors using an extended Kalman filter for rotor resistance sensorless estimation" IEEE Transactions on energy conversion, Vol.15, no.1, pp. 66-70, March 2000.
[6]. HARKATI Nacereddine, HAOUD Lahcen, "Determination of the parameters of the asynchronous machine taking into account thermal, film and saturation effects". PFE in Electrotechnics, ENP of Algiers, year 2009.

BIBLIOGRAPHY

Kabimba Mupa . Diploma from Master's degree 2017 University of Brazzaville-Congo and PhD student in engineering sciences of The University of Brazzaville-Congo.

Prof.Dr.Ir Lidinga Mobonda Flory , PhD In Engineering Sciences, Dept. Of Electricity.
ENSP-UMNG Electrical Engineering Research Laboratory.
Teacher-Researcher at ISTA-Boma

MA.Dr.Ir , **Leonide Messo** . PhD In Engineering Sciences, Dept. Of Electricity.
ENSP-UMNG Electrical Engineering Research Laboratory
Teacher-Researcher at ENSP

Prof.Dr.Ir Narcisse Meni Babaka , Ph.D. University Michoacana of San Nicolas of Hidalgo (UMSNH) Mexico 2021,
Teacher-Researcher at ISTA-Kinshasa

Prof.Dr.Ir André Bandekela Kazadi , is an electrical engineer, he received his PhD, from the energetic institute of Moecou (Rusie). Director of the ISTA-Kin doctoral school

Prof.Dr.Ir Desire LILONGA BOENGA
presently lecturer at the University of Brazzaville-Congo, Dept. Electronics.
Teacher-Researcher at ENSP